Journal of The Electrochemical Society, **152** (7) J65-J73 (2005)
0013-4651/2005/152(7)/J65/9/$7.00 © The Electrochemical Society, Inc.

Electrical Conductivity and Oxygen Nonstoichiometry of $La_{0.2}Sr_{0.8}Fe_{0.55}Ti_{0.45}O_{3-\delta}$

Chan Young Park* **and Allan J. Jacobson****,z**

Center for Material Chemistry, Department of Chemistry, University of Houston, Houston, Texas 77204-5003, USA

The electrical conductivity of $La_{0.2}Sr_{0.8}Fe_{0.55}Ti_{0.45}O_{3-\delta}$ (LSFTO) was measured in the temperature range $750 \leqslant T \leqslant 1000$°C and at oxygen partial pressures of $1 \times 10^{-18} \leqslant p_{O_2} \leqslant 0.3$ atm. The conductivity was measured on both increasing and decreasing p_{O_2} to ensure that equilibrium was reached. Long equilibration times were required at intermediate oxygen partial pressures between 10^{-4} and 10^{-11} atm. The pressure dependence of the conductivity in this p_{O_2} range differs from that previously reported for related compositions. The mobilities of the charge carriers were derived from the stoichiometry and conductivity data. The average hole and electron mobilities of LSFTO at $800 \leqslant T \leqslant 1000$°C are 0.015 and 0.0017 $cm^2\ V^{-1}\ s^{-1}$, respectively. The oxygen nonstoichiometry (δ) as a function of p_{O_2} was determined by solid-state coulometric titration. Data were obtained in the temperature range, $750 \leqslant T \leqslant 1040$°C, and in the p_{O_2} range, $10^{-17} \leqslant p_{O_2} \leqslant 0.3$ atm. A point defect model was used to fit the dependence of δ on p_{O_2}. The partial molar thermodynamic quantities for oxidation were calculated and the oxygen nonstoichiometry data were related to the electrical conductivity data.
 [DOI: 10.1149/1.1931307]

Manuscript submitted December 23, 2004; revised manuscript received January 27, 2005. Available electronically June 10, 2005.

Mixed ionic electronic conductors (MIECs) with the ABO_3 perovskite or related structures have been widely studied because of their practical applications in ion-transport membranes, pressure-driven oxygen generators, partial oxidation reactors, and as electrodes for solid oxide fuel cells (SOFCs).[1,2] As discussed previously, the $La_{1-x}Sr_xFeO_{3-\delta}$ (LSFO) series has high mixed conductivity[3] and better stability than the $La_{1-x}Sr_xCoO_{3-\delta}$ (LSCO) series but still exhibits limited stability in low-p_{O_2} environments. The analogous iron-cobalt series has also been extensively studied. According to Teraoka *et al.*, for $La_xSr_{1-x}Co_yFe_{1-y}O_{3-\delta}$ (LSCFO), the ionic and electronic conductivities are on the order of 0.01-1.0 S cm^{-1} and $\geqslant$100 S cm^{-1} at 800°C, respectively.[4] Electrochemical studies of the mixed conducting oxides, $La_{1-x}M_xCo_{1-y}Fe_yO_{3-\delta}$ (M = Sr, Ba, Ca) and an electrical conductivity relaxation study of $La_{0.6}Sr_{0.4}Fe_{0.8}Co_{0.2}O_{3-\delta}$ have been reported.[5,6]

The titanium-substituted compositions, $SrTi_{1-x}Fe_xO_{3-\delta}$ (STFO), have a relatively high level of mixed conductivity with an ionic conductivity of ~0.2 S cm^{-1} at 1000°C.[7-9] Unfortunately, relatively high thermal expansion coefficients (TECs) and poor stability both in highly reducing conditions and with respect to reaction with yttria-stabilized zirconia (YSZ) limit their use. Lanthanum substitution on the A-site, $La_{1-x}Sr_xFe_{1-y}Ti_yO_{3-\delta}$, solves some of these problems.[8-11] The stability and mixed conducting properties of LSFTO compositions were studied by Fagg *et al.*,[9] but only a limited amount of information is available. In this paper, we report the four-probe dc and ac conductivities (σ) of $La_{0.2}Sr_{0.8}Fe_{0.55}Ti_{0.45}O_{3-\delta}$ at different oxygen partial pressures p_{O_2} and the oxygen nonstoichiometry (δ) determined by solid-state coulometric titration. The results provide information relevant to the practical applications of the material in ion-transport membrane reactors.

Experimental

$La_{0.2}Sr_{0.8}Fe_{0.55}Ti_{0.45}O_{3-\delta}$ (LSFTO) powder, synthesized by using the spray pyrolysis method, was obtained from Praxair Specialty Ceramics (Woodinville, WA). The powder was preheated at 1250°C for 10 h in air with a 3°C/min ramp rate. The preheated powder was ground with ethanol in a mortar for more than 30 min. After drying to remove the ethanol, the powder was pressed into a cylindrical shape at 5000 psi with a 1 in. diam die. Dense ceramic disks were obtained by sintering in air at 1300°C for 20 h and 1400°C for 10 h. The sintered disks had a density of ~90.3% of the theoretical density measured using the Archimedes method. Phase purity, chemical analysis, and chemical homogeneity of the sample were determined by using X-ray powder diffraction (Scintag XDS 2000), electron microprobe analysis (JEOL JXA-8600), and scanning electron microscopy (JEOL JSM-6330F).

The dc four-probe method was used to determine the conductivity at $25 \leqslant T \leqslant 900$°C and $5 \times 10^{-5} \leqslant p_{O_2} \leqslant 1$ atm. Gold wire contacts were made to a rectangular bar with dimensions 9.02 × 2.54 × 1.91 mm. The electrical conductivity and oxygen nonstoichiometry (δ) as a function of p_{O_2} were determined by using gas-tight electrochemical cells. The details of the method can be found elsewhere but are briefly summarized here.[12,13]

Polycrystalline yttria-stabilized zirconia (YSZ-8) disks were prepared using 8 mol % Y_2O_3-doped zirconia powder (TOSOH zirconia, TZ-8Y, TOSOH Corp.). The powder was pressed uniaxially into disks which were cold isostatically pressed at 40,000 psi and then sintered at 1450°C for 4 h. Pt paste (Engelhard 6926) was painted on both faces of the YSZ-8 disks. Pt wires (0.0025 cm diam) were connected to the YSZ by using Pt meshes (150 × 150 mesh, 0.005 cm wire diam, Unique Wire Weaving Co., Inc.).

The electrochemical cell for conductivity measurements was built by stacking alumina rings [outside diameter (o.d.) = 12 mm, thickness = 1.5 mm, and height = 3-10 mm] and Pyrex glass rings (o.d. = 12 mm, thickness = 1.5 mm, and height = 0.5-1 mm) one by one. Both the top and the bottom of the cell were closed with YSZ-8 disks. The YSZ-8 disks were used as sensors to monitor p_{O_2} inside the cell with air as the reference gas on the outside. One YSZ cell was used intermittently as a pump in order to control the oxygen flux into the cell and thereby the p_{O_2}. Four Pt wires were linked to the rectangular sample bar that was placed in the middle of the cell. The Pt wires inside the cell were brought out through the glass rings. The cell became gas-tight when the temperature was raised above 821°C and the glass rings softened. The electromotive force (emf) of the sensor was measured by using a Keithley 2000-20 multimeter. A Keithley 2400 SourceMeter was used as the pump current source. The experiments were controlled by Labview software through a general purpose interface bus (GPIB) communicator. The coulometric titration experiments were carried out in a similar though simpler cell, because the additional seals used to bring out the conductivity leads are not needed.

To minimize the current flow through the sample, an ac four-point probe technique was used to monitor the conductivity of the sample with a lock-in amplifier (Stanford Research Systems, model SR 830 DSP). The lock-in amplifier enabled us to measure very low voltages without noise problems.

The dimensions of two samples used for the conductivity mea-

* Electrochemical Society Student Member.
** Electrochemical Society Active Member.
z E-mail: ajjacob@uh.edu

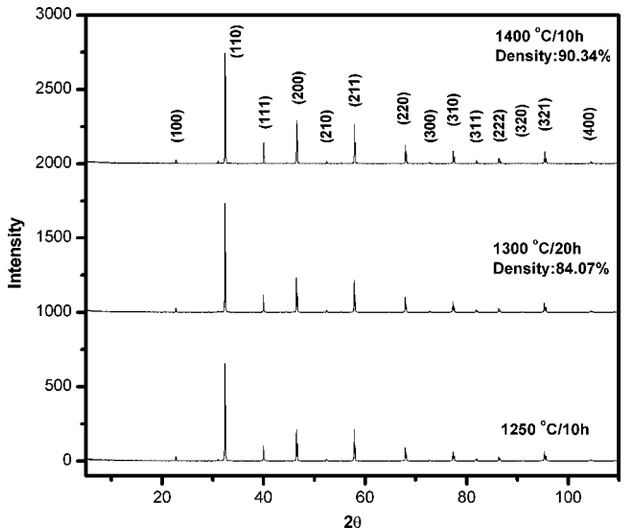

Figure 1. The XRD patterns for $La_{0.2}Sr_{0.8}Fe_{0.55}Ti_{0.45}O_{3-\delta}$ samples annealed at different temperatures.

surements were $2.92 \times 1.78 \times 10.29$ mm and $2.79 \times 1.57 \times 9.53$ mm. The p_{O_2} dependences of the conductivity were measured in the ranges at $750 \leqslant T \leqslant 1000$°C and $10^{-18} \leqslant p_{O_2} \leqslant 0.3$ atm. The criterion for equilibrium used was that the conductivity changed by less than 0.0002 S cm^{-1} min^{-1} and, importantly in the intermediate p_{O_2} region, the time was chosen such that the p_{O_2} gradient between the top and bottom sensors was small (less than half an order of magnitude), which is an even more stringent criterion. In this region, each point took at least 6 h before the p_{O_2} criterion was met. The standard approach to establishing equilibrium by approaching from both directions was used. The δ values were determined by coulometric titration in the ranges $750 \leqslant T \leqslant 1040$°C and $10^{-17} \leqslant p_{O_2} \leqslant 0.3$ atm. In these experiments, about 0.2-0.5 g of LSFTO powder was used. A change in sensor voltage less than 0.04%/min was used as the criterion for equilibrium. The variation of the stoichiometry of the sample was recorded as a function of temperature at $25 \leqslant T \leqslant 900$°C and $p_{O_2} = 0.1$ atm with a 2°C/min of ramp rate using a TA Instruments Hi-Res 2950 system. The thermogravimetric analysis (TGA) results were compared to dc conductivity data and the normalized δ values from the coulometric titration experiment.

Results

Characterization.— The LSFTO powder was calcined at a series of temperatures (1250, 1300, and 1400°C) in air to investigate phase purity and densification behavior. X-ray diffraction (XRD) powder patterns are shown in Fig. 1. The sample is single phase after heating at 1250°C. At the higher sintering temperatures, the lines become sharper and the density increases. The density measured by the Archimedes method was 90.3% relative to theoretical value after annealing at 1400°C for 10 h. The XRD pattern sintered at 1400°C was completely indexed with a cubic unit cell with lattice parameter $a = 3.898(8)$ Å and $V = 59.2(6)$ $Å^3$. The weak XRD peaks at ~31, 43, 55, and 65° 2θ are also from the perovskite phase and arise from a small amount of W_L radiation in the incident beam.

The final sintered specimen was mounted and polished in epoxy (ME14730 epoxy resin and epoxy hardener) for electron microprobe analysis (EMPA, JEOL JXA-8600). The backscattered electron image shown in Fig. 2a confirmed a homogeneous single phase of LSFTO. Elemental compositions were determined with the probe placed at several different spots on the sample. The composition ratios were determined from the average data to be La:Sr = 0.196(1):0.804(8) and Fe:Ti = 0.550(4):0.450(4), in agreement with the nominal composition. The detailed analysis results are presented in Table I. According to the XRD and EPMA results, the sample is more than 99% homogeneous with no apparent secondary phases. Scanning electron microscopy (SEM, JEOL JSM-6330F) was used to investigate the grain size, grain distribution, and surface morphology of the sample (Fig. 2b). The grain size of the sample is ⩽10 μm.

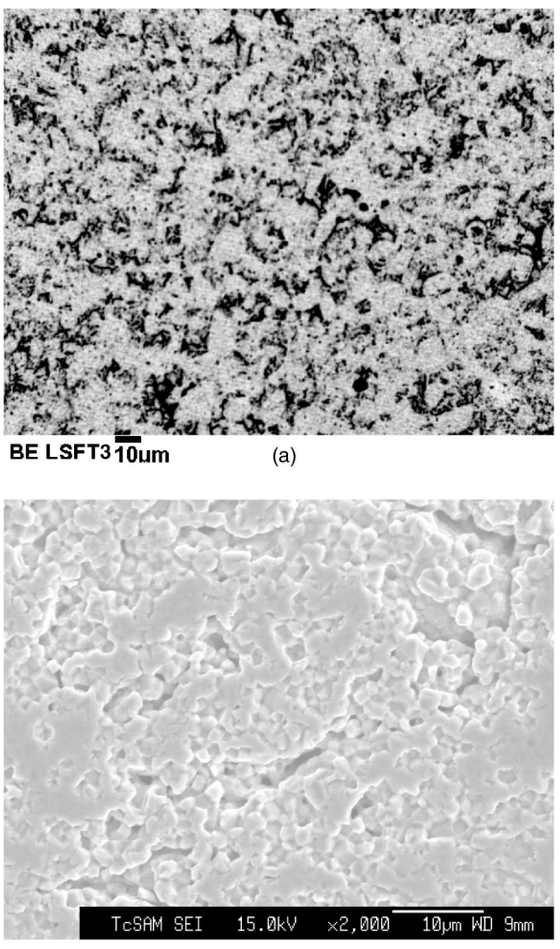

Figure 2. (a) Backscattered electron image and (b) SEM micrograph of $La_{0.2}Sr_{0.8}Fe_{0.55}Ti_{0.45}O_{3-\delta}$ sintered at 1400°C/10 h.

Table I. The composition of $La_{0.2}Sr_{0.8}Fe_{0.55}Ti_{0.45}O_{3-\delta}$ determined by EPMA.

Point no.	Atom %				
	La	Sr	Fe	Ti	O
1	3.948	16.104	11.567	9.412	58.970
2	3.961	16.522	11.695	9.475	58.348
3	3.977	16.338	11.560	9.615	58.510
4	3.979	16.181	11.673	9.553	58.614
5	4.021	16.331	11.749	9.634	58.265
Average	3.977	16.295	11.649	9.538	58.541
S.D.	0.028	0.161	0.083	0.094	0.276
Composition	0.196(1)	0.804(8)	0.550(4)	0.450(4)	3.00-δ

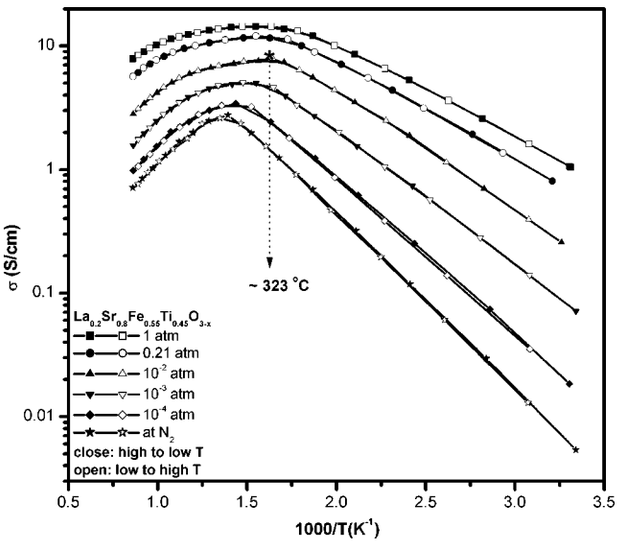

Figure 3. The four-probe dc conductivity of $La_{0.2}Sr_{0.8}Fe_{0.55}Ti_{0.45}O_{3-\delta}$ from p_{O_2} = 1 to 10^{-4} atm. Closed symbols correspond to the measurements from high to low temperature and open marks correspond from low to high.

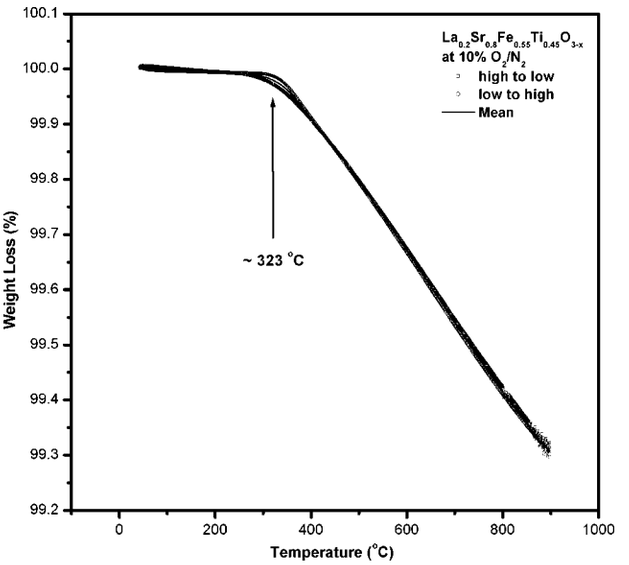

Figure 4. TGA data for $La_{0.2}Sr_{0.8}Fe_{0.55}Ti_{0.45}O_{3-\delta}$ at 0.1 atm.

Conductivity.— The temperature dependence of the total conductivity (σ) of LSFTO at $\sim 5 \times 10^{-5} \leqslant p_{O_2} \leqslant 1$ atm and $25 \leqslant T \leqslant 900$°C is shown in Fig. 3. All measurements were made on both heating and cooling with the condition that equilibrium was assumed to be reached when the conductivity changed by less than 0.0005 S cm^{-1} min^{-1}. At temperatures lower than ~320°C, all plots are close to linear, with the conductivity increasing with increasing temperature. The activation energies (E_a) are in the range of 0.14-0.28 eV and are similar in magnitude to previously reported activation energies for other electronically conducting perovskite systems. A summary of activation energies is given in Table II.

The activation energies for the electronic conductivity increase with decreasing p_{O_2} as the contribution from the ionic conductivity to the total conductivity increases. The maximum conductivity observed in p_{O_2} = 1 atm is ~14 S cm^{-1} at ~400°C. Above 400°C, the conductivity falls as the temperature increases due to the decrease of the concentration of electron holes as the concentration of oxygen vacancies increases at elevated temperatures according to Eq. 1[5]

Table II. Activation energies for $La_{0.2}Sr_{0.8}Fe_{0.55}Ti_{0.45}O_{3-\delta}$ at low temperatures.

Composition	p_{O_2} (atm)	E_a (ev)	Ref.
$La_{0.2}Sr_{0.8}Fe_{0.55}Ti_{0.45}O_{3-\delta}$	1	0.14(5)	This work
	0.21	0.15(4)	This work
	10^{-2}	0.18(5)	This work
	10^{-3}	0.21(1)	This work
	10^{-4}	0.25(0)	This work
	10^{-5}	0.28(0)	This work
$La_{0.4}Sr_{0.6}Fe_{0.4}Ti_{0.6}O_{3-\delta}$	0.21	0.42(7)	9
$La_{0.4}Sr_{0.6}Fe_{0.6}Ti_{0.4}O_{3-\delta}$	0.21	0.25(5)	9
$La_{0.4}Sr_{0.6}Fe_{0.8}Ti_{0.2}O_{3-\delta}$	0.21	0.27(7)	9
$La_{0.4}Sr_{0.5}Fe_{0.4}Ti_{0.6}O_{3-\delta}$	0.21	0.29(5)	9
$La_{0.2}Sr_{0.8}Fe_{0.4}Ti_{0.6}O_{3-\delta}$	0.21	0.34(0)	9
$La_{0.2}Sr_{0.7}Fe_{0.4}Ti_{0.6}O_{3-\delta}$	0.21	0.35(1)	9
$La_{0.5-x}Sr_{0.5-x}Fe_{0.4}Ti_{0.6}O_{3-\delta}$ (x = 0.02–0.10)	0.21	0.24~0.26	8

$$2Fe_{Fe}^{\bullet} + O_O^x \rightarrow [V_O^{\bullet\bullet}] + 2Fe_{Fe}^x + \frac{1}{2}O_2 \qquad [1]$$

The conductivities of LSFTO at different partial pressures of oxygen were extracted from the dc conductivities. The conductivities systematically increase with increasing p_{O_2}, indicating that the compound is a p-type conductor in this p_{O_2} region. At 900°C, the slope of the log-log plot is ~1/4 as expected. As the temperature decreases, the slopes decrease until they reach a value of ~1/6 at 500°C. Data obtained at lower p_{O_2} are discussed below.

The change in weight as a function of temperature at $25 \leqslant T \leqslant 900$°C and p_{O_2} = 0.1 atm is shown in Fig. 4. The weight change is reversible on heating and cooling. The temperature at which oxygen loss begins to occur is ~320°C, in agreement with the temperature at which the conductivity decreases (Fig. 3). Stevenson *et al.* reported similar TGA behavior for $(La,Sr)(Co,Fe)O_{3-\delta}$.[6] The TGA data were used to cross-check the normalization of the coulometric titration data (see below).

The electrical conductivity measurements were made in a sealed electrochemical cell as a function of p_{O_2} at temperatures from 750 to 1000°C down to 10^{-18} atm for the lowest temperature. The measurements were made using an ac four-point technique at a single frequency (1 kHz) and the phase angle monitored to confirm the absence of any polarization effects. The isothermal plots measured on both decreasing and increasing p_{O_2} are shown in Fig. 5. The data are typical for perovskite oxides. The conductivity initially is p-type at high oxygen partial pressure and decreases as p_{O_2} decreases. In the high-p_{O_2} region ($10^{-6} \leqslant p_{O_2} \leqslant 0.3$ atm), the total conductivity (σ_T) decreased with increasing temperature because the concentration of electron holes increases with decreasing temperature. The slopes of the linear region in a log-log plot are ~1/4($\sigma \propto p_{O_2}^{1/4}$).

In the range between $10^{-10} \leqslant p_{O_2} \leqslant 10^{-7}$ atm, the conductivity becomes dominated by the ion and electron contributions and the isotherms switch over so that the highest conductivity corresponds to the highest temperature. Consequently, the conductivity isotherms converge to a similar value in the middle-p_{O_2} range. A small change in slope is observed most noticeably in the higher temperature data. This reason for this discontinuity will be discussed in a separate paper. As the p_{O_2} is further decreased, the conductivity goes through a minimum and then becomes n-type with a $\sigma \propto p_{O_2}^{-1/4}$ depen-

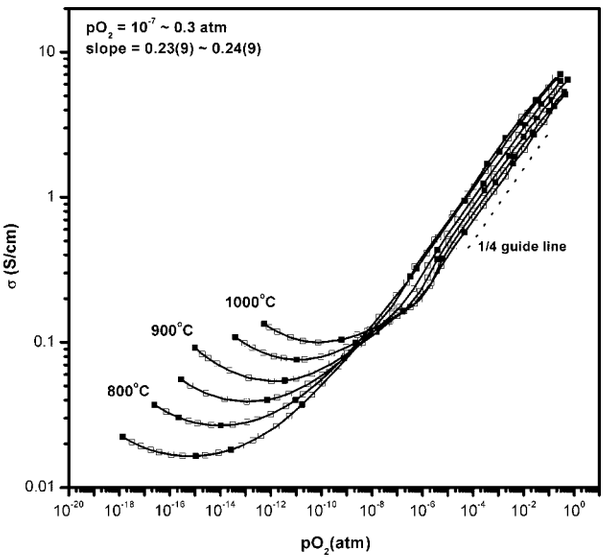

Figure 5. Conductivity measurements for $La_{0.2}Sr_{0.8}Fe_{0.55}Ti_{0.45}O_{3-\delta}$ as a function of p_{O_2} at different temperatures. Open and closed symbols represent data taken on increasing and decreasing p_{O_2}.

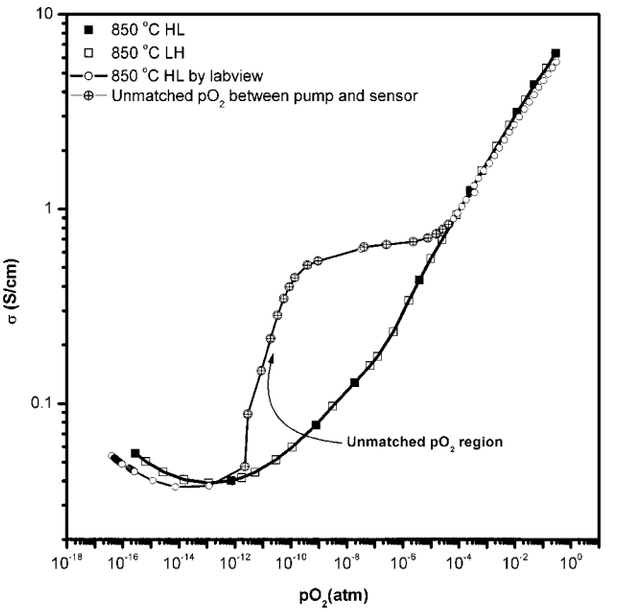

Figure 6. Comparison of two different conductivity measurements as a function of p_{O_2} for $La_{0.2}Sr_{0.8}Fe_{0.55}Ti_{0.45}O_{3-\delta}$ at 850°C. Open circles represent data taken using the equilibrium criterion ($\leqslant$0.0005 S cm^{-1} min^{-1}).

dence. The conductivity minima occur between $10^{-15} \leqslant p_{O_2} \leqslant 10^{-10}$ atm and move to lower p_{O_2} as the temperature decreases (Table III).

The criterion for attainment of equilibrium was carefully investigated because long equilibration times were observed, especially in the range of $10^{-12} \leqslant p_{O_2} \leqslant 10^{-5}$ atm. Three criteria for attainment of equilibrium were used. Over most of the p_{O_2} regions, equilibrium was assumed when the conductivity changed by $\leqslant$0.0002 S cm^{-1} min^{-1}, and the values of p_{O_2} measured by the sensors at the top and bottom of the cell differed by less than a half order of magnitude. In the middle-p_{O_2} region, this criterion was insufficient and longer times (typically 6 h per data point) were needed to ensure that the p_{O_2} gradient was less than a half order of magnitude. With these criteria, good agreement between data measured both on increasing and on decreasing p_{O_2} was obtained.

These results can be contrasted with results obtained using a less stringent equilibrium criterion of $\leqslant$0.0005 S cm^{-1} min^{-1} as shown in the open circle data in Fig. 6. A large discrepancy is observed in the middle-p_{O_2} region. A difference between the measured values of p_{O_2} by the sensors at the top and bottom of the cell of more than one order of magnitude in p_{O_2} was found under these conditions. In general, the p_{O_2} difference between the two sensors is slow to converge due to the slow equilibrium kinetics and consequently, both conductivity and log p_{O_2} difference criteria are needed to ensure that equilibrium is reached. The open circle data in Fig. 6 are similar to results in other ferrite perovskite oxides and reflect nonequilibrium behavior.[14-17]

Table III. Results of the conductivity minima and p_{O_2} at p-n transition region.

Temp.(°C)	1000/T (K^{-1})	p_{O_2}	σ_{min} (S/cm)	Log $\sigma_{min}T$
750	0.977	1.16×10^{-15}	0.0158 ± 0.0001	1.21
800	0.932	9.18×10^{-15}	0.0258 ± 0.0001	1.44
850	0.890	2.06×10^{-13}	0.0376 ± 0.0001	1.63
900	0.852	7.09×10^{-13}	0.0514 ± 0.0001	1.78
950	0.817	1.24×10^{-11}	0.0724 ± 0.0002	1.95
1000	0.785	1.07×10^{-10}	0.0935 ± 0.0002	2.08

Stoichiometry.— The oxygen nonstoichiometry (δ) for LSFTO was measured as a function of p_{O_2} at 750 $\leqslant T \leqslant$ 1040°C. Measurements were made in a sealed electrochemical cell at $10^{-16} \leqslant p_{O_2} \leqslant$ 0.3 atm. About 0.2-0.5 g of powder was used and measurements made on both decreasing and increasing p_{O_2}. The relative δ-values were measured as a function of p_{O_2} and then corrected for the leakage through the 8 mol % YSZ cell. The leakage is more significant at higher temperature and at lower p_{O_2}. The details of the leakage correction procedure were described previously.[12,13] The minimum value of $\partial\delta/\partial p_{O_2}$ is taken to indicate the stoichiometric composition of the sample at this p_{O_2}.[18,19] For $La_{0.2}^{3+}Sr_{0.8}^{2+}Fe_{0.55}^{3+}Ti_{0.45}^{4+}O_{3-\delta}$, an inflection in the titration data indicates that $\delta \cong 0.175$. One ex-

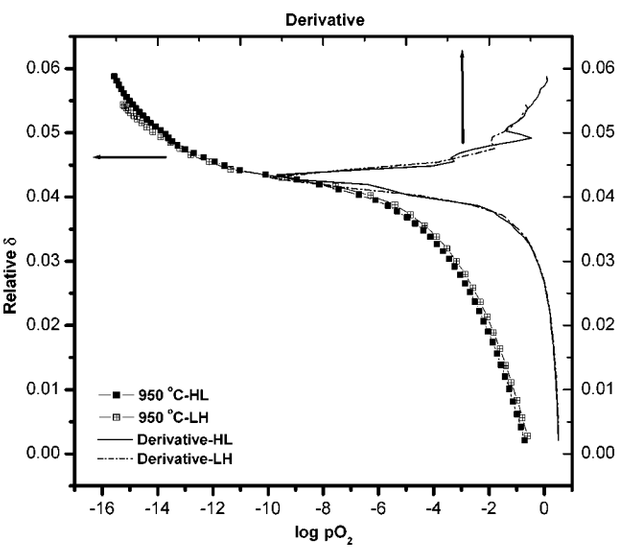

Figure 7. Determination of stoichiometric composition by using the minimum value of $\partial\delta/\partial p_{O_2}$ for $La_{0.2}Sr_{0.8}Fe_{0.55}Ti_{0.45}O_{3-\delta}$ at 950°C.

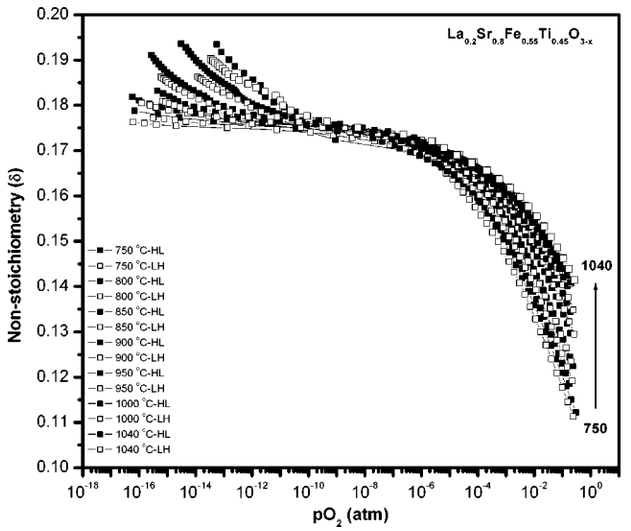

Figure 8. The p_{O_2} dependence of average oxygen nonstoichiometry (δ) measured on increasing and decreasing p_{O_2} for $La_{0.2}Sr_{0.8}Fe_{0.55}Ti_{0.45}O_{3-\delta}$.

ample measured at 950°C is shown in Fig. 7. The solid line in this graph is $\partial\delta/\partial p_{O_2}$. The minimum value of $\partial\delta/\partial p_{O_2}$ at 950°C occurred at $p_{O_2} \approx 8.3 \times 10^{-11}$ and 3.2×10^{-10} atm for high to low and low to high p_{O_2} measurements, respectively. Excellent agreement between the conductivity minima and the stoichiometric condition extracted from Fig. 7 is found.

The absolute δ-values were obtained with this assumption and the other data points were normalized. The change in normalized δ-values from 750 to 900°C at 0.1 atm is consistent with the TGA results after the latter are corrected for buoyancy. Results for the variation of the oxygen nonstoichiometry are shown in Fig. 8. The experimental results display good reproducibility irrespective of the p_{O_2} direction of measurement. The δ-values increased almost linearly on lowering p_{O_2} until they approached the ideal stoichiometric composition, $\delta = 0.175$. A plateau is observed between $p_{O_2} \approx 10^{-12}$ and 10^{-7} atm. The p_{O_2} corresponding to the ideal stoichiometry moves to higher p_{O_2} as the temperature increases. Then, the δ-values increase again on further lowering p_{O_2}. A small difference between the high to low and low to high data was observed in this region that was most apparent at $p_{O_2} \leqslant 10^{-13}$ atm and at $T \geqslant 1000$°C. The total changes in δ were less than ~0.1 at the p_{O_2} and temperatures measured. All measurements covered the whole p_{O_2} range except for the low-p_{O_2} values at 750°C where equilibrium times were too long.

Discussion

Defect model.— A simple point defect model is used to analyze the p_{O_2} dependence of the oxygen nonstoichiometry. The predominant defect species are assumed to be $V_O^{\bullet\bullet}$ (oxygen vacancy, δ), $Fe_{Fe}^{\bullet} = Fe^{4+}$, $Fe_{Fe}' = Fe^{2+}$, and Sr_{La}',[20] and $Ti_{Fe}^{\bullet}$. Here, defects are expressed in Kröger-Vink notation[21] and $LaFeO_3$ is chosen as a standard reference state. This point defect model assumes random noninteracting defects and only doubly ionized oxygen vacancies.

The oxygen incorporation reaction between oxygen gas and defects in LSFTO is given by

$$\frac{1}{2}O_2(g) + V_O^{\bullet\bullet} + 2Fe_{Fe}^{x} = O_O^{x} + 2Fe_{Fe}^{\bullet} \quad [2]$$

where Fe_{Fe}^{x} and O_O^{x} are Fe^{3+} ion and O^{2-} ion on the lattice sites, respectively. The equilibrium constant (K_{ox}) for the reaction is

$$K_{ox} = \frac{[O_O^{x}][Fe_{Fe}^{\bullet}]^2}{p_{O_2}^{1/2}[V_O^{\bullet\bullet}][Fe_{Fe}^{x}]^2} = \frac{(3-\delta)[Fe_{Fe}^{\bullet}]^2}{p_{O_2}^{1/2}\delta[Fe_{Fe}^{x}]^2} \quad [3]$$

The Fe^{3+} ions (Fe_{Fe}^{x}) undergo charge-disproportionation into Fe^{2+} (Fe_{Fe}') and Fe^{4+} ($Fe_{Fe}^{\bullet}$)

$$2Fe_{Fe}^{x} = Fe_{Fe}' + Fe_{Fe}^{\bullet} \quad [4]$$

The equilibrium constant is given by

$$K_D = \frac{[Fe_{Fe}^{\bullet}][Fe_{Fe}']}{[Fe_{Fe}^{x}]^2} \quad [5]$$

In addition, site relations and the electroneutrality condition provide three more equations

$$[Fe_{Fe}^{x}] + [Fe_{Fe}^{\bullet}] + [Fe_{Fe}'] = 0.55 \quad [6]$$

$$[V_O^{\bullet\bullet}] + [O_O^{x}] = 3 \quad [7]$$

$$[Sr_{La}'] + [Fe_{Fe}'] = [Ti_{Fe}^{\bullet}] + 2[V_O^{\bullet\bullet}] + [Fe_{Fe}^{\bullet}] \quad [8]$$

where $[Sr_{La}'] = 0.8$ and $[Ti_{Fe}^{\bullet}] = 0.45$. Some abbreviations will be used for simplicity: $V_O^{\bullet\bullet}$ (=δ), $Fe_{Fe}^{\bullet} = Fe^{4+}$ (=p), $Fe_{Fe}' = Fe^{2+}$ (=n), and $Fe_{Fe}^{x} = Fe^{3+}$ (=a). Under oxidizing p_{O_2} atmospheres, $[Fe_{Fe}^{x}]$ and $[Fe_{Fe}^{\bullet}]$ are much greater than $[Fe_{Fe}']$. Therefore, Eq. 6 and 8 can be rewritten as

$$a + p = 0.55 \quad [9]$$

$$0.35 = p + 2\delta \quad [10]$$

The equilibrium constant K_{ox} can be expressed with respect to the measurable parameters, p_{O_2} and δ

$$K_{ox} = \frac{(3-\delta)p^2}{p_{O_2}^{1/2}\delta a^2} = \frac{(3-\delta)(0.35-2\delta)^2}{p_{O_2}^{1/2}\delta(0.2+2\delta)^2} \quad [11]$$

On decreasing p_{O_2}, $[Fe_{Fe}^{\bullet}]$ becomes small and the p value in Eq. 10 can be ignored, hence $0.35 \cong 2\delta$. At $\delta = 0.175$, the concentrations of holes and electrons is theoretically the same (see Fig. 9a). The equilibrium constant (K_D) in Eq. 5 is given in terms of p_{O_2}, δ, and K_{ox} by

$$K_D = \frac{[Fe_{Fe}^{\bullet}][Fe_{Fe}']}{[Fe_{Fe}^{x}]^2} = \frac{np}{a^2} = \frac{p^2}{a^2} = \frac{K_{ox}pO_{O_2}^{1/2}\delta}{3-\delta} \quad [12]$$

In the most reducing conditions, the hole concentration can be neglected and hence, Eq. 8 can be simplified to

$$0.35 + n \cong 2\delta \quad [13]$$

Alternatively, the K_D value can be calculated in terms of p and δ by the combination of Eq. 6, 8, and 12

$$K_D = \frac{(p + 2\delta - 0.35)p}{(0.9 - 2p - 2\delta)^2} \quad [14]$$

Equation 14 can be rearranged with respect to give the hole concentration (p) in terms of K_D. Once the hole concentration (p) is known, a and n values can be calculated by using Eq. 6-8.

Table IV. The calculated model parameters at different temperatures.

Temperature(°C)	1000/T (K^{-1})	K_{ox}	K_D
800	0.932	4.37	4.96×10^{-7}
850	0.890	3.25	7.93×10^{-7}
900	0.852	2.15	1.45×10^{-6}
950	0.818	1.55	2.68×10^{-6}
1000	0.785	1.16	4.35×10^{-6}

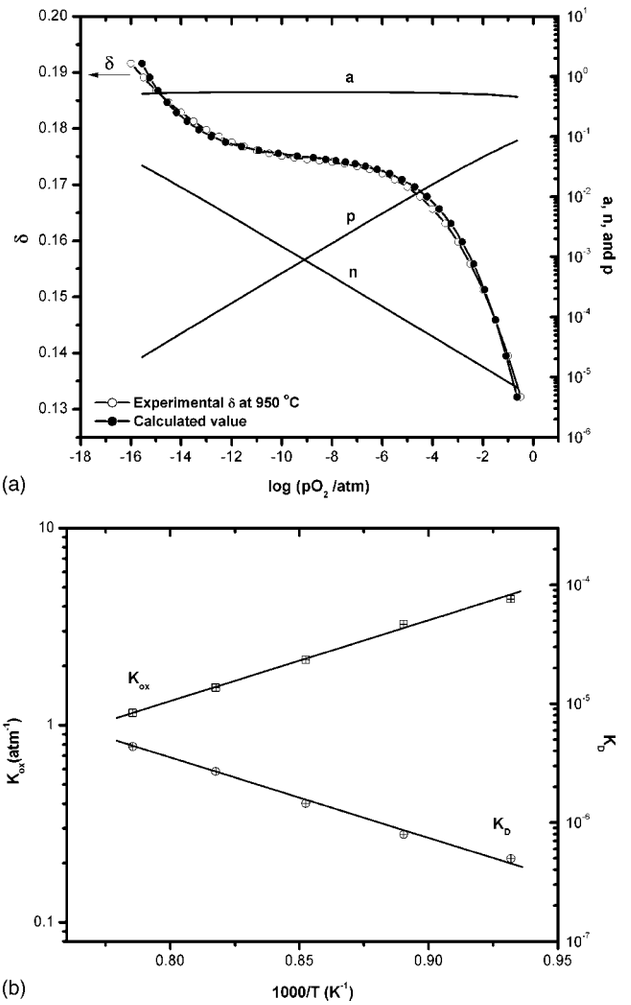

Figure 9. (a) The calculated concentrations of defect species, δ, *a*, *n*, and *p*, and (b) the Arrhenius plots of K_{ox} and K_D for $La_{0.2}Sr_{0.8}Fe_{0.55}Ti_{0.45}O_{3-\delta}$ at 950°C.

The p_{O_2} dependences of *a* ($=Fe_{Fe}^{x}$), *n* ($=Fe_{Fe}^{\prime}$), and *p* ($=Fe_{Fe}^{\bullet}$) for LSFTO at 950°C are shown in Fig. 9a. The oxygen vacancy concentrations (δ) calculated by using Eq. 2-8 are in good agreement with the experimental values. As expected, *p* increases with increasing p_{O_2} and vice versa for *n* and Fe_{Fe}^{x} ($=a$) is nearly constant over the entire range of p_{O_2}. Values of K_{ox} and K_D at 950°C of 1.55 and 2.68×10^{-6}, respectively, were obtained.

The values K_{ox} and K_D calculated using this point defect model at $800 \leqslant T \leqslant 1000$°C are summarized in Table IV. The calculated δ values are in good agreement with the experimental values for all measured temperatures. The temperature dependence of K_{ox} and K_D is shown in Fig. 9b. The values of K_{ox} increase as the temperature decreases and the K_D values show the opposite trend. Based on the data in Fig. 9b, the standard enthalpy of the reaction (Eq. 3), ΔH_{OX}°, and Eq. 5, ΔH_{D}°, can be obtained from

$$\Delta G_{OX}^{\circ} = \Delta H_{OX}^{\circ} - T\Delta S_{OX}^{\circ} = -RT \ln K_{OX} \quad [15]$$

$$\Delta G_{D}^{\circ} = \Delta H_{D}^{\circ} - T\Delta S_{D}^{\circ} = -RT \ln K_{D} \quad [16]$$

The calculated values of ΔH_{OX}° and ΔH_{D}° for LSFTO were −77.4 and 125.8 kJ/mol, respectively. Per mole of iron atoms, ΔH_{OX}° and ΔH_{D}° are −140.7 and 228.7 kJ/mol, respectively. The value of ΔH_{D}° (228.7 kJ/mol = 2.37 eV) is related to the bandgap of LSFTO. Ionic (σ_i) and electron conductivities (σ_e) as well as activation energies (E_a) for related compositions are summarized in Table V.

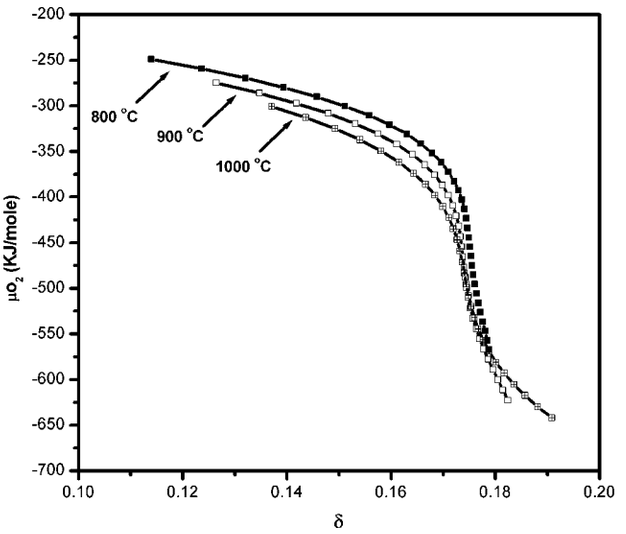

Figure 10. The calculated partial molar free energies of oxygen (μ_{O_2}) as a function of δ for $La_{0.2}Sr_{0.8}Fe_{0.55}Ti_{0.45}O_{3-\delta}$.

Thermodynamics.— The partial molar free energies of oxygen, (μ_{O_2}), at equilibrium between the solid and the gas phases were calculated by using the following equation

$$\mu_{O_2,solid} = \mu_{O_2,gas} = \mu(0)_{O_2,gas} + RT \ln p_{O_2} \quad [17]$$

where $\mu_{O_2,solid}$ and $\mu_{O_2,gas}$ are the chemical potentials of oxygen in the solid and of the gas, respectively. Also, $\mu(0)_{O_2,gas}$ is the chemical potential of the gas in the standard state, $p_{O_2} = 1$ atm. The values of the chemical potential of the gas in standard state, $[\mu(0)_{O_2,gas}]$, are temperature dependent and were reported by Lankhorst *et al.*[22]

$$\mu(0)_{O_2,gas} = RT\left[n_1 + n_2\frac{1}{T} + n_3 \ln(T) + n_4 \ln\left\{1 - \exp\left(-\frac{n_5}{T}\right)\right\}\right] \quad [18]$$

where $n_1 = -1.225$, $n_2 = -1.045 \times 10^3$ K, $n_3 = -3.500$, $n_4 = 1.013$, and $n_5 = 2.242 \times 10^3$ K. The calculated values of μ_{O_2} as a

Table V. The ionic and electron conductivities of some oxides.

Compounds	Temp.(°C)	σ_i (S/cm)	E_a (eV)	σ_e (S/cm)	E_a (eV)	Ref.
10% YSZ	1000	~0.1	0.74			7
$La_{0.3}Sr_{0.7}FeO_{3-\delta}$	900	~0.26	0.80	5.4×10^{-5}	2.35	15
$La_{0.3}Sr_{0.7}Fe_{0.9}Ga_{0.1}O_{3-\delta}$	900	~0.15	0.78			16
$Sr_{0.97}Ti_{0.6}Fe_{0.4}O_{3-\delta}$	900	~0.04	1.01			7
$La_{0.2}Sr_{0.8}Fe_{0.55}Ti_{0.45}O_{3-\delta}$	900	~0.035	0.63	1.0×10^{-5}	2.40	This work

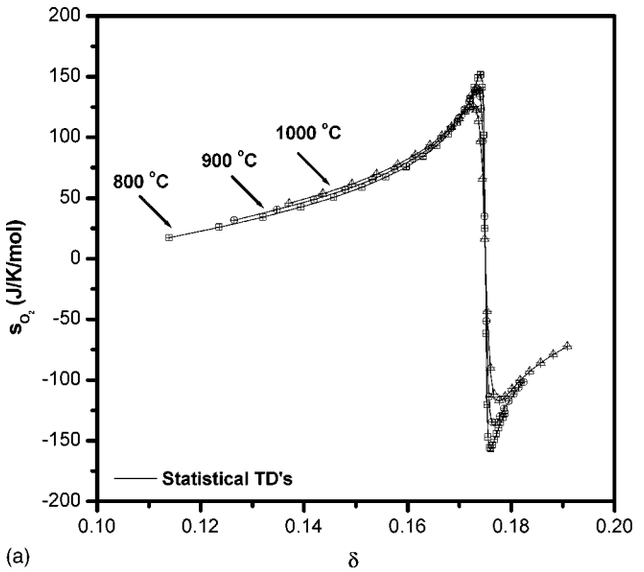

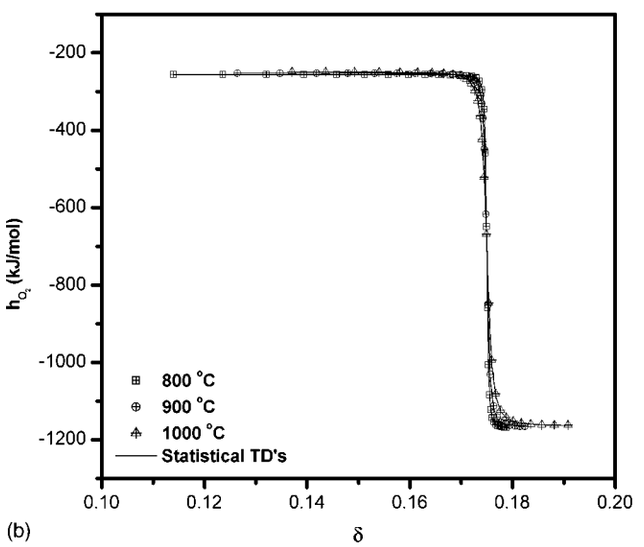

Figure 11. (a) The calculated partial molar entropy of oxygen (s_{O_2}) and (b) the calculated partial molar enthalpy of oxygen (h_{O_2}) as a function of δ for $La_{0.2}Sr_{0.8}Fe_{0.55}Ti_{0.45}O_{3-\delta}$. Symbols are calculated by the Gibbs-Helmholtz equation. Lines correspond to the partial molar quantities calculated by statistical thermodynamics.

function of δ based on the coulometric titration data are shown in Fig. 10. The calculations were made in the temperature ranges of $800 \leqslant T \leqslant 1000$°C. The slopes of all curves gradually decreased as δ increased and abruptly dropped around near the ideal stoichiometric δ due to the rapid decrease in the partial molar entropy (s_{O_2}). Also, the values of μ_{O_2} became more negative with increasing temperature.

The partial molar enthalpy (h_{O_2}) and the partial molar entropy (s_{O_2}) of oxygen can be derived from the chemical potential (μ_{O_2}) of oxygen as below

$$\mu_{O_2} = h_{O_2} + Ts_{O_2} \qquad [19]$$

$$s_{O_2} = -\frac{\partial \mu_{O_2}}{\partial T} \text{ and } h_{O_2} = \frac{\partial (\mu_{O_2}/T)}{\partial (1/T)} \qquad [20]$$

The partial molar entropy of oxygen (s_{O_2}) was calculated by using Eq. 20. The partial molar entropy as a function of δ in the range of $800 \leqslant T \leqslant 1000$°C is shown in Fig. 11a. The partial molar entropy shows a very small dependence on temperature and increases from ~25 J/K/mol at $\delta \approx 0.12$ to ~150 J/K/mol at $\delta \approx 0.17(4)$. The abrupt drop in s_{O_2} at $\delta \cong 0.175$ is due to the decrease in configurational entropy ($s_{O,conf.}$), the main contribution to s_{O_2}, at the stoichiometric point.[20] The variation of the partial molar enthalpy as a function of δ in the same temperature is shown in Fig. 11b. The partial molar enthalpy is related to the standard enthalpy of Reaction 2 and for ideal behavior, $h_{O_2} = 2\Delta H^{\circ}_{OX}$.[23] Values in the range $0.12 \leqslant \delta \leqslant 0.17$ are almost constant, suggesting no significant interactions among point defects and drop abruptly near $\delta \approx 0.175$.

The configurational entropy ($s_{O,conf.}$) can be determined by using a model proposed by Mizusaki.[20,24] The configurational entropy, partial molar enthalpy, and partial molar entropy can be expressed in terms of δ, *a*, *n*, and *p* values as follows

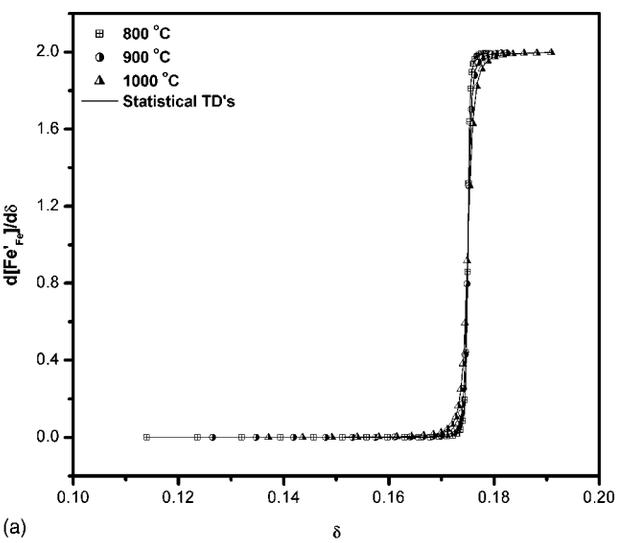

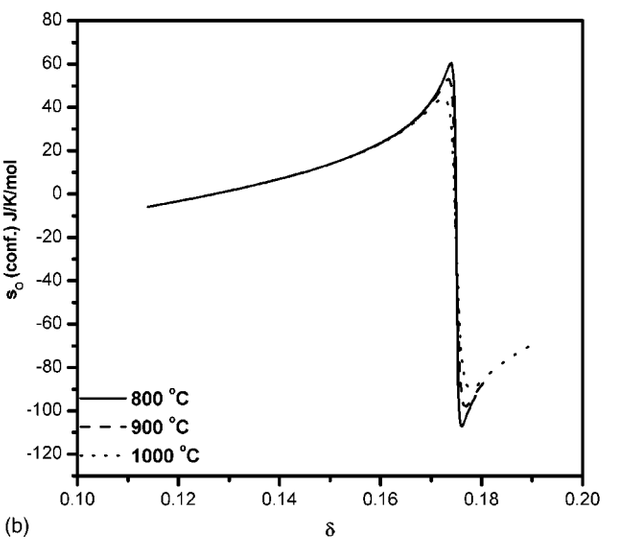

Figure 12. (a) The plots of $\partial[Fe'_{Fe}]/\partial\delta$ *vs.* δ and (b) s_o *vs.* δ for LSFTO. Symbols are calculated by the Gibbs-Helmholtz equation. Lines correspond to the partial molar quantities calculated by statistical thermodynamics.

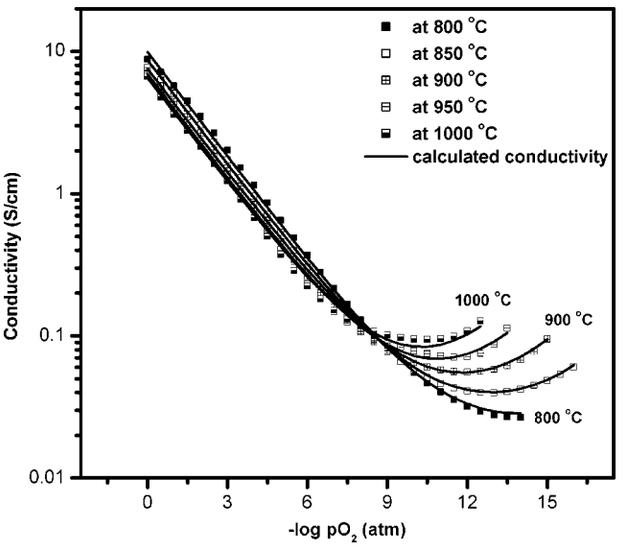

Figure 13. The calculated conductivities of $La_{0.2}Sr_{0.8}Fe_{0.55}Ti_{0.45}O_{3-\delta}$ as a function of δ at 750 ≤ *T* ≤ 1000 °C.

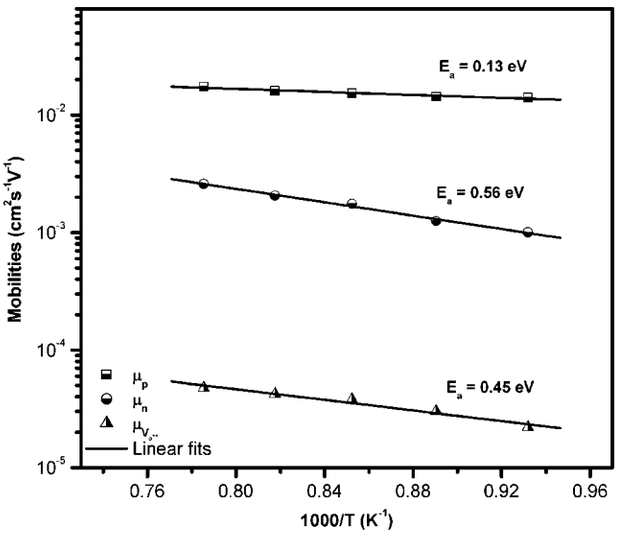

Figure 14. Temperature dependence of the defect mobilities for $La_{0.2}Sr_{0.8}Fe_{0.55}Ti_{0.45}O_{3-\delta}$.

$$s_{O_2,conf} = 2s_{O.conf} = 2R\left(\ln\frac{\delta a^2}{(3-\delta)p^2}\right) + \frac{\partial n}{\partial \delta}\ln K_D \quad [21]$$

$$\frac{1}{2}(h_{O_2} - h^\circ_{O_2}) = (h_O - h^\circ_O) = \Delta H^\circ_{OX} - \frac{\partial n}{\partial \delta}\Delta H^\circ_D \quad [22]$$

$$\frac{1}{2}(s_{O_2} - s^\circ_{O_2}) = (s_O - s^\circ_O) = \Delta S^\circ_{OX} - \frac{\partial n}{\partial \delta}\cdot\Delta S^\circ_D + s_{O,conf.} \quad [23]$$

where $V_O^{\bullet\bullet}$ (=δ), $Fe_{Fe}^{\bullet}$ (=*p*), Fe_{Fe}' (=*n*), and Fe_{Fe}^{x} (=*a*). The values of the configurational entropy increase from ~0 J/K/mol at δ ≅ 0.12 to ~60 J/K/mol at δ ≅ 0.17(4). The trend of $s_{O,conf.}$ indicated with the solid lines reflects the variation of the partial molar entropy of oxygen (s_O) with respect to δ. Similar results showing this general behavior of $s_{O,conf.}$ were reported previously for $La_{0.6}Sr_{0.4}FeO_{3-\delta}$ and $La_{0.4}Sr_{0.6}FeO_{3-\delta}$.[20]

The partial molar entropy and enthalpy were calculated from Eq. 21 and 22 using

$$\frac{\partial [Fe_{Fe}']}{\partial \delta} = 1 + \frac{2\delta - 0.35}{4K_d[Fe_{Fe}^{\times}] + [Fe_{Fe}^{\bullet}] + [Fe_{Fe}']} \quad [24]$$

Figure 12a shows these results. The configurational entropies ($s_{O,conf.}$), shown in Fig. 12b, were calculated by inserting Eq. 24 into Eq. 21. The calculated partial molar quantities are in good agreement with the experimental values (Fig. 11).

Conductivity.—The p_{O_2} dependence of the conductivity data can be analyzed to extract the mobilities by using the defect concentrations from the p_{O_2} dependence of the stoichiometry. The conductivity can be written

$$\sigma = \frac{F(p\mu_p + n\mu_n + 2\delta\mu_{V_O^{\bullet\bullet}})}{V_m} \quad [25]$$

where *F* and V_m are Faraday constant and molar volume of LSFTO, respectively. The mobilities, μ_p, μ_n, and $\mu_{V_O^{\bullet\bullet}}$ were obtained by least-squares fitting the data to Eq. 25 with the assumption that the mobilities are constant. The calculated conductivities are shown in Fig. 13 and agree well with the experimental data. The mobilities of the electron holes, electrons, and oxygen ions have activation energies of 0.13, 0.56, and 0.45 eV, respectively (Fig. 14). The mobilities of electrons and oxygen ions slightly increased as temperature is increased, whereas the hole mobilities are weakly dependent on temperature. The average hole and electron mobilities of LSFTO between 800 and 1000°C are 0.015 and 0.0017 $cm^2\ V^{-1}\ s^{-1}$. According to previous reports for $LaFeO_3$, μ_h = 0.107 $cm^2\ V^{-1}\ s^{-1}$ and μ_e = 0.056 $cm^2\ V^{-1}\ s^{-1}$ [25] and for $La_{0.75}Sr_{0.25}FeO_3$ μ_h = 0.09 $cm^2\ V^{-1}\ s^{-1}$ and μ_e = 0.07 $cm^2\ V^{-1}\ s^{-1}$.[26] The values of μ_h and μ_e of LSFTO are about one order of magnitude lower, presumably due to the large concentration of titanium atoms on the perovskite B sites.

Conclusions

The electrical conductivity properties of $La_{0.2}Sr_{0.8}Fe_{0.55}Ti_{0.45}O_{3-\delta}$ were studied by four-probe dc and ac electrical conductivity measurements using gas-sealed electrochemical cells. In the intermediate pressure range, the equilibration kinetics are very slow and reproducible data on both increasing and decreasing p_{O_2} can be obtained only by using long equilibration times. This effect is observed for other iron-containing perovskites and its origin is under investigation.

The p_{O_2} dependence of oxygen nonstoichiometry (δ) was determined by using coulometric titration. The data were analyzed using a simple point defect model and thermodynamic quantities were calculated. From this model, the standard enthalpy for oxidation (ΔH°_{OX}) and disproportionation (ΔH°_D) were determined to be −140.7 and 228.7 kJ/mol, respectively. The mobilities of the electron holes, electrons, and oxygen ions were calculated from the conductivity data using the defect concentrations determined from the stoichiometry and point defect model.

Acknowledgments

The work was supported by the Department of Energy, DOE-DE-FC26-99FT40054, and the Robert A. Welch Foundation. The support by Praxair is also gratefully acknowledged.

The University of Houston assisted in meeting the publication costs of this article.

References

1. H. J. M. Bouwmeester and A. J. Burggraaf, *The CRC Handbook of Solid State Electrochemistry*, P. J. Gellings and H. J. M. Bouwmeester, Editors, p. 481, CRC Press, Boca Raton, FL (1997).
2. E. L. Brosha, R. Mukundan, D. R. Brown, F. H. Garzon, J. H. Visser, M. Zanini, Z. Zhou, and E. M. Logothetis, *Sens. Actuators B*, **69**, 171 (2000).
3. J. H. Yoo, C. Y. Park, and A. J. Jacobson, *Solid State Ionics*, **175**, 55 (2004) .
4. Y. Teraoka, H. Zhang, K. Okamoto, and N. Yamazoe, *Mater. Res. Bull.*, **23**, 51

(1988).
5. S. Wang, P. A. W. van der Heide, C. Chaves, A. J. Jacobson, and S. B. Alder, *Solid State Ionics*, **156**, 201 (2003).
6. J. W. Stevenson, T. R. Armstrong, R. D. Carneim, L. R. Pederson, and W. J. Weber, *J. Electrochem. Soc.*, **143**, 2722 (1996).
7. V. V. Kharton, A. P. Viskup, A. V. Kovalevsky, J. R. Jurado, E. N. Naumovich, A. A. Vecher, and J. R. Frade, *Solid State Ionics*, **133**, 57 (2000).
8. D. P. Fagg, J. C. Waerenborgh, V. V. Kharton, and J. R. Frade, *Solid State Ionics*, **146**, 87 (2002).
9. D. P. Fagg, V. V. Kharton, J. R. Frade, and A. A. L. Ferreira, *Solid State Ionics*, **156**, 45 (2003).
10. V. V. Kharton, F. M. Figueiredo, A. V. Kovalevsky, A. P. Viskup, E. N. Naumovich, J. R. Jurado, and J. R. Frade, *Defect Diffus. Forum*, **186-187**, 119 (2000).
11. D. P. Fagg, V. V. Kharton, A. V. Kovalevsky, A. P. Viskup, E. N. Naumovich, and J. R. Frade, *J. Eur. Ceram. Soc.*, **21**, 1831 (2001).
12. J. Yoo, A. Verma, and A. J. Jacobson, in *Ionic and Mixed Conducting Ceramics IV*, T. A. Ramanarayanan, W. L. Worrell, and M. Mogensen, Editors, PV 2001-28, p. 27, The Electrochemical Society Proceedings Series, Pennington, NJ (2001).
13. J. Yoo and A. J. Jacobson, in *Solid-State Ionic Devices III*, E. D. Wachsman, M.-L. Liu, M. F. Carolan, F. H. Garzon, K. Swider-Lyons, and S. R. Setter, Editors, PV 2002-26 p. 354, The Electrochemical Society Proceedings Series, Pennington, NJ (2003).
14. V. L. Kozhevnikov, I. A. Leonidov, M. V. Patrakeev, E. B. Mitberg, and K. R. Poeppelmeier, *J. Solid State Chem.*, **158**, 320 (2000).
15. I. A. Leonidov, V. L. Kozhevnikov, M. V. Patrakeev, E. B. Mitberg, and K. R. Poeppelmeier, *Solid State Ionics*, **144**, 361 (2001).
16. I. A. Leonidov, V. L. Kozhevnikov, E. B. Mitberg, M. V. Patrakeev, V. V. Kharton, and F. M. B. Marques, *J. Mater. Chem.*, **11**, 1201 (2001).
17. M. V. Patrakeev, J. A. Bahteeva, E. B. Mitberg, I. A. Leonidov, V. L. Kozhevnikov, and K. R. Poeppelmeier, *J. Solid State Chem.*, **172**, 219 (2003).
18. C. Wagner, *Prog. Solid State Chem.*, **6**, 1 (1971).
19. J. Mizusaki, M. Yoshihiro, S. Yamauchi, and K. Fueki, *J. Solid State Chem.*, **58**, 257 (1985).
20. J. Mizusaki, M. Yoshihiro, S. Yamauchi, and K. Fueki, *J. Solid State Chem.*, **67**, 1 (1987).
21. F. A. Kröger and H. J. Vink, *Solid State Phys.*, **3**, 307 (1956).
22. M. H. R. Lankhorst, H. J. M. Bouwmeester, and H. Verweij, *J. Solid State Chem.*, **133**, 555 (1997).
23. O. T. Sørensen, *Nonstoichiometric Oxides*, O. T. Sørensen, Editor, pp. 1–59, Academic Press, New York (1981).
24. J. Mizusaki, S. Yamauchi, K. Fueki, and A. Ishikawa, *Solid State Ionics*, **12**, 119 (1984).
25. J. Mizusaki, T. Sasamoto, W. R. Caccon, and H. K. Bowen, *J. Am. Ceram. Soc.*, **65**, 363 (1982).
26. J. Mizusaki, T. Sasamoto, W. R. Caccon, and H. K. Bowen, *J. Am. Ceram. Soc.*, **66**, 247 (1983).